ACS Photonics

Open Access

This article is licensed under CC-BY-NC-ND 4.0

pubs.acs.org/journal/apchd5

Article

Tempering Multichannel Photon Emission from Emitter-Coupled Holographic Metasurfaces

Published as part of ACS Photonics virtual special issue "Frontiers and Applications of Plasmonics and Nanophotonics".

Yinhui Kan,* Xujing Liu, Shailesh Kumar, and Sergey I. Bozhevolnyi*

Cite This: *ACS Photonics* 2024, 11, 1584–1591

Read Online

ACCESS | Metrics & More | Article Recommendations | Supporting Information

ABSTRACT: On-chip manipulation of photon emission from quantum emitters (QEs) is crucial for quantum nanophotonics and advanced optical applications. At the same time, the general design strategy is still elusive, especially for fully exploring the degrees of freedom of multiple channels. Here, the vectorial scattering holography (VSH) approach developed recently for flexibly designing QE-coupled metasurfaces is extended to tempering the strength of QE emission into a particular channel. The VSH power is demonstrated by designing, fabricating, and optically characterizing on-chip QE sources emitted into six differently oriented propagation channels, each representing the entangled state of orthogonal circular polarizations with different topological charges and characterized with a specific relative strength. We postulate that the demonstration of tempered multichannel photon emission from QE-coupled metasurfaces significantly broadens the possibilities provided by the holographic metasurface platform, especially those relevant for high-dimensional quantum information processing.

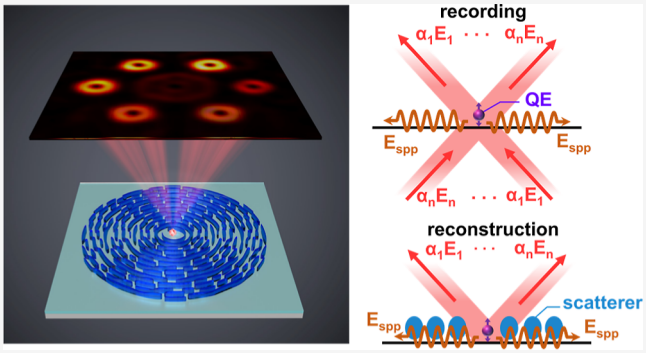

KEYWORDS: *metasurfaces, quantum emitter, holography, multichannel, surface plasmon polariton, nanodiamond*

INTRODUCTION

Engineering characteristics of radiation from quantum emitters (QEs) is crucial for quantum technologies as typical free-standing QEs feature poorly defined directivity, polarization, and wavefronts.[1−6] Conventional approaches for shaping photon emission rely on bulky optical components and systems, such as wave plates, lens, polarizers, and spatial light modulators, complicated arrangements that unavoidably increase the system complexity and lower the efficiency of photon emission.[7−12] Recently, on-chip QE-coupled metasurfaces, consisting of arrayed nanostructures integrated with QEs, have been proposed to efficiently outcouple QE-excited (nonradiative) surface plasmon polaritons (SPPs) into well-defined photon emission,[13−19] opening thereby a new avenue, which is different from previously developed external metasurfaces[20−24] or individual nanostructures.[25−32] On-chip (at-source) generation of single-photon emission with radial and circular polarizations (RP and CP) has been realized with QE-coupled bullseye nanoridges[14] and width-gradient nanoridges,[15] respectively. Encoding single-photon beams with orbital angular momentum was demonstrated with Archimedean spiral nanoridge gratings that can be set with different number of arms related to the topological charges.[16] Furthermore, on-chip generation of single-photon circularly polarized single-mode vortex beams[33] and linearly polarized vortex beams[34] have been realized with QE-coupled anisotropic metasurfaces by arranging carefully designed anisotropic elements into appropriate surface patterns.[33,34]

The general design strategy exploited is based on the vectorial scattering holography (VSH), which can be viewed as an inverse design approach and that was recently proposed for designing metasurfaces to structure QE photon emission into a well-collimated stream of photons with desired polarizations.[35] The VSH application has resulted in significant progress comparing with previous directional but poorly polarized photon emission that was generated simply with QE-coupled Doppler bullseye nanoridges.[17] Very recently, the VSH design strategy has been applied to realize on-chip integrated efficient generation of two well-collimated single-photon beams

Received: November 29, 2023
Revised: January 30, 2024
Accepted: January 31, 2024
Published: February 15, 2024

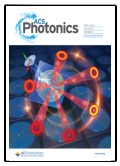

© 2024 The Authors. Published by American Chemical Society

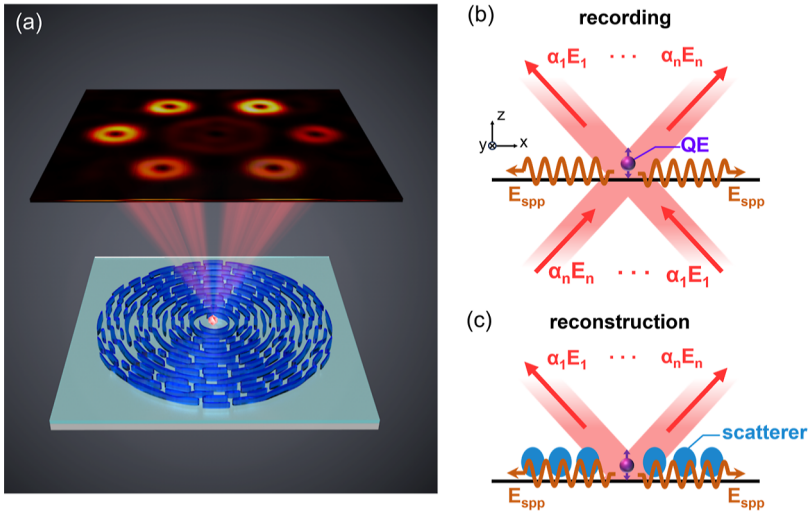

Figure 1. On-chip QE-coupled holography metasurfaces for tempering photon emission into multiple channels. (a) Schematic of on-chip QE-coupled holography metasurfaces for generation of directional photon emission with different intensities in each channel. (b,c) Process of designing on-chip QE-coupled metasurfaces with developed holography approach, (b) recording process of the interference between QE-excited SPPs (i.e., reference waves) and multiple signal waves with different directions, polarizations, and amplitudes, (c) reconstruction process by coupling QE-excited SPPs into photon emission with holography metasurfaces composed of nanoscatterers.

propagating along different off-normal directions with orthogonal linear polarizations, a complex functionality that can be assigned to a chip-integrated micronano single-photon polarization beam splitter.[36] Moreover, the original VSH approach[35] has further been extended and applied to realize quantum light sources for multichannel emission encoded with different spin and orbital angular momenta in each channel, extending multiple degrees of freedoms of QE radiation.[37] Although these studies demonstrated a very powerful platform for on-chip manipulation of photon emission, on-chip generation of multichannel photon emission with different intensities in each channel has not yet been realized, and the corresponding design approach is still elusive.

In this work, we further develop the VSH for structuring multichannel photon emission propagating along different directions so that the QE emission strength in each channel can flexibly be tempered by using preset signal waves in the VSH procedure. To show the versatility of the developed approach, we designed, fabricated, and characterized a set of holographic metasurfaces that on-chip couple with nitrogen-vacancy (NV) centers in nanodiamonds (NDs). The photon emission, which is radially polarized and can be decomposed in to left- and right-hand circular polarization (LCP and RCP), propagating in six channels with the identical azimuthal angle (20°) is demonstrated. Similarly, we realize the generation of six-channel photon emission propagating in two sets of different zenith angles (10 and 20°). Furthermore, we demonstrate the generation of photon emission with gradually adjusted intensity in different channels, a demonstration that enables more freedom for on-chip structuring of QE radiation with implications to advanced optical applications and quantum technologies.

RESULTS AND DISCUSSION

The generic implementation of on-chip QE-coupled holographic metasurfaces for tempering photon emission into multiple channels with different intensities is schematically shown in Figure 1a. A properly selected QE (i.e., featuring a dominant radiative dipole perpendicular to the surface plane)[14−17] is found atop a 20 nm thin SiO_2 spacer covering a silver (Ag) film. When the QE is driven by a strongly focused radially polarized excitation laser beam, radially polarized SPPs are QE-excited and radially propagate along the substrate surface. By introducing a properly designed metasurface, composed of nanoscatterers positioned around the QE, the QE-excited SPPs would be coupled into free-space photon emission with desired properties. Like in the classical holography approach,[38] the developed VSH should first be applied to generate the surface hologram, which is then binarized end up in a metasurface nanoridge structure. Notably, it is the in-plane nonradiative QE-excited SPPs that are utilized as reference waves, $\boldsymbol{E}_{spp}$, in the recoding process (Figure 1b), a feature that is crucially different from those inherent to classical holography approach.[38] Multiple (N) signal waves, $\boldsymbol{E}_{s,n}$, with arbitrary directions (zenith angle θ_n and azimuthal angle φ_n), polarizations (e.g., RP or CP), and amplitude ratios (α_n), are applied to interfere with the reference wave, $\boldsymbol{E}_{spp}$, thus generating the interference pattern (i.e., a hologram), $I(x, y) = \sum_{n=1}^{N} |\boldsymbol{E}_{spp} + \alpha_n \boldsymbol{E}_{s,n}|^2$. It is important to generate the total interference pattern from the superposition of individual interference patterns that are related to each channel with independent properties, rather than obtaining a combined interference pattern resulting from the interference between the superimposed (multiple) signal waves and reference wave. The latter may result in an unwanted crosstalk and diffusely scattered light.[37] Furthermore, by properly setting a threshold, the interference pattern can be binarized into nanoridge structures (holographic metasurfaces) that are to be fabricated around the QE and utilized to reconstruct the photon emission with the desired channel amplitudes, corresponding to the preset signal waves, by outcoupling the QE-excited SPP waves (Figures 1c, S1 and Note S1).

Here, we use the hydrogen silsesquioxane (HSQ), one of the dielectric polymers whose refractive index is 1.41,[39] to construct the metasurfaces. The thickness of the metasurfaces is 180 nm. With the filling ratio set as 0.5, the effective refractive index is about 1.24. The inner and outer radii of the

https://doi.org/10.1021/acsphotonics.3c01745
ACS Photonics 2024, 11, 1584−1591

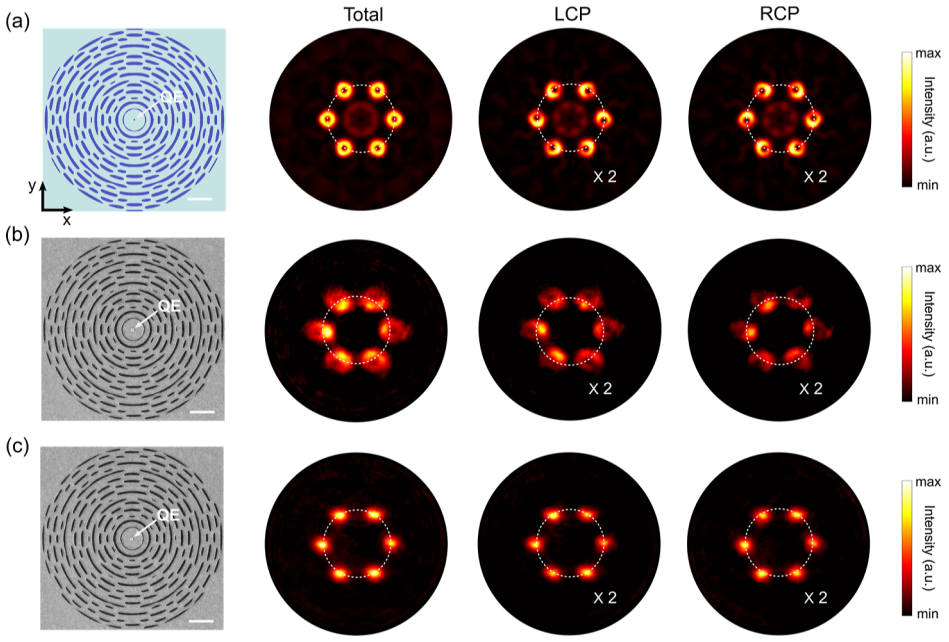

Figure 2. Structuring photon emission into multichannel off-normal directions with the identical azimuthal angle by on-chip QE-coupled holography metasurfaces. (a) Simulation results of the generation of photon emission propagation with the zenith angle of $\theta = 20°$ and azimuthal angles of $\varphi_1 = 0°$, $\varphi_2 = 60°$, $\varphi_3 = 120°$, $\varphi_4 = 180°$, $\varphi_5 = 240°$, and $\varphi_6 = 300°$. From left to right: the configuration (scale bar, 2 μm), the emission pattern (NA = 0.9), the LCP component, and the RCP component, where the dashed circles indicate the emission angle of $\theta = 20°$. (b) Experimental results with a bandpass filter of 676 ± 15 nm. From the left to the right: the SEM image of the sample (scale bar, 2 μm), the emission pattern (NA = 0.9), the LCP component, and the RCP component. (c) Experimental result with a bandpass filter of 650 ± 20 nm.

metasurfaces are set to be 0.75 and 7 μm, respectively, which is able to efficiently outcouple the nonradiative QE-excited SPPs into free space photon emission. It is possible to further optimize the metasurface configuration by carefully taking into account the beam size of signal wave and the SPP propagation loss during the interference process of holography[35] and thus balance the structure size and the outcoupling efficiency. In this work, we use the ND-NV centers as QEs whose emission peaks are around λ = 670 nm when operating at room temperature and being driven by 532 nm laser.[14,15] It should be noted that the proposed approach is general that can be used for different kinds of QEs, such as quantum dots, molecules, defects in 2D materials, and other color centers in diamonds, with different decay rates and emission wavelengths.[40−43] Moreover, the material of metasurfaces is also not limited to HSQ, other dielectric materials,[44−46] e.g., TiO_2, can be used to construct the designed metasurfaces.

The signal waves include six radially polarized beams with corresponding propagation angles, which can be expressed as $\boldsymbol{E}_{s,n} = (\boldsymbol{E}_{sx,n}; \boldsymbol{E}_{sy,n}) \sim \exp(-ik_0\boldsymbol{r}_{s,n})\cdot\exp(il_n\varphi)\cdot(\cos\varphi; \sin\varphi)$, where $\boldsymbol{r}_{s,n} = \sin\theta_n \cos\varphi_n\cdot x + \sin\theta_n \sin\varphi_n\cdot y$, $\varphi = \tan^{-1}(y/x)$, and $k_0 = 2\pi/\lambda$. In this work, for simplicity, the topological charges of signal waves are set as 0, $l_n = 0$. We start from the relatively simple regime for off-normal photon emission with the zenith angle of $\theta = 20°$ and the azimuthal angles (clockwise) of $\varphi_1 = 0°$, $\varphi_2 = 60°$, $\varphi_3 = 120°$, $\varphi_4 = 180°$, $\varphi_5 = 240°$, and $\varphi_6 = 300°$, where the amplitudes of six signal waves are identical (i.e., $|\boldsymbol{E}_{s,1}| = |\boldsymbol{E}_{s,2}| = |\boldsymbol{E}_{s,3}| = |\boldsymbol{E}_{s,4}| = |\boldsymbol{E}_{s,5}| = |\boldsymbol{E}_{s,6}|$). The signal waves independently interfere with the reference wave, i.e., the QE excited nonradiative SPPs radially propagating on the surfaces, which is in the form of $\boldsymbol{E}_{spp} \sim \exp(-ik_{spp}\cdot\boldsymbol{r})\cdot(\cos\varphi; \sin\varphi)$, where the radius vector $\boldsymbol{r} = \sqrt{x^2 + y^2}$, $k_{spp} = (2\pi/\lambda)N_{spp}$, with N_{spp} being the effective index of SPPs at the targeted wavelength λ of photon emission from QEs. The holography metasurface is binarized from the total interference pattern and then integrated with the QE. Three-dimensional (3D) finite difference time domain (FDTD) simulations are conducted to characterize the performance of the designed QE-coupled holography metasurfaces, where the QE is treated as an electrical dipole (λ = 670 nm) vertically orientated to the substrate surfaces. As shown in Figure 2a, from the left to the right are the configuration of the metasurface, the emission pattern, the LCP component, and the RCP component (NA = 0.9). The photon emission in each channel propagates exactly in the corresponding angles as theoretically designed (indicated with the dashed white lines). Due to the intrinsic properties of radially polarized QE-excited SPPs, the reconstructed photon emission can be decomposed into LCP (with topological charge of −1) and RCP (with topological charge of +1) components where the total angular momentum is conserved.[37] Evolution of generation of photon emission from a single channel to multiple channels can be found in Figure S2. Furthermore, to experimentally demonstrate the design strategy, we fabricated the designed holography metasurfaces (made of HSQ) precisely around the preselected NDs containing NV centers that are treated as QEs on top of the silica-covered silver film, following the well-developed fabrication process[15] (Figure S3). Figure 2b shows the scanning electron microscopy (SEM) image of the fabricated sample and the characterization photon emission (NA = 0.9) with a bandpass filter of 676 ± 15 nm being used to filter a narrow band photon emission around the emission peak (Figure S4), which coincides well with the simulation results. Moreover, the radial polarization property of the photon emission is characterized by rotating a polarizer (details can be found in Figure S5). It should be noted that the ND-NVs are

https://doi.org/10.1021/acsphotonics.3c01745
ACS Photonics 2024, 11, 1584−1591

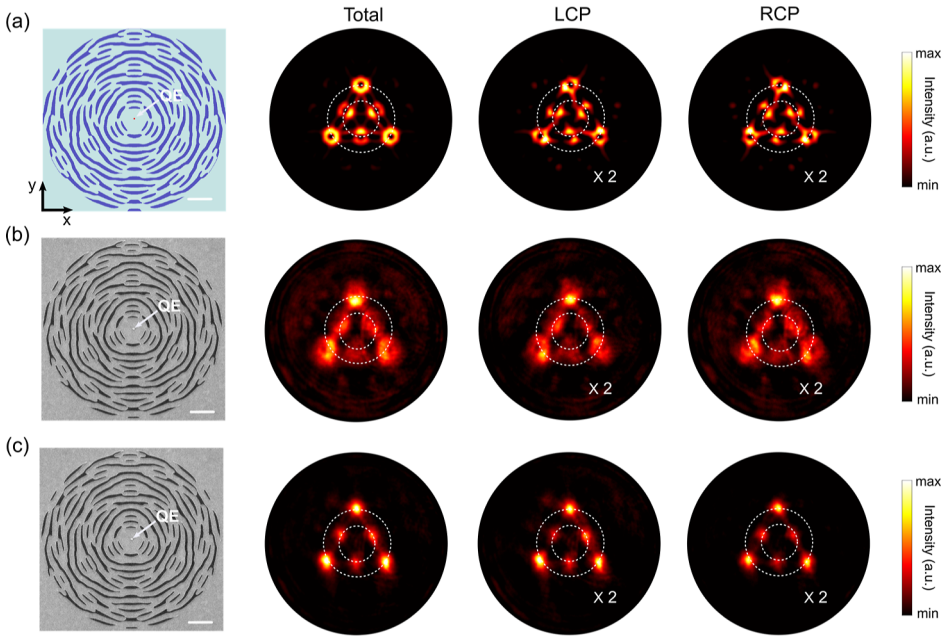

Figure 3. Structuring photon emission into multichannel off-normal directions with two set of different zenith angles by on-chip QE-coupled holography metasurfaces. (a) Simulation results of the generation of photon emission propagating with angles of $\theta_1 = 20°$ and $\theta_2 = 10°$, and the azimuthal angles of $\varphi_1 = 30°$, $\varphi_2 = 90°$, $\varphi_3 = 150°$, $\varphi_4 = 210°$, $\varphi_4 = 270°$, and $\varphi_6 = 330°$, respectively. From left to right: the configuration (scale bar, 2 μm), the emission pattern (NA = 0.9), the LCP component, and the RCP component. (b) Experimental results with a bandpass filter of 676 ± 15 nm. From left to right: the SEM image of the sample (scale bar, 2 μm), the emission pattern (NA = 0.9), the LCP component, and the RCP component. (c) Experimental result with a bandpass filter 650 ± 20 nm.

driven by a tightly focused radially polarized 532 nm laser beam, in which the horizontal (in-plane) components can be canceled by each other in the focal spot, thus leading to a large vertical (out-of-plane) component of the electric field. Thus, the QEs feature the radiative transition dipoles dominant with their large vertical excitation components perpendicular to the surface.[15] Moreover, we also checked the performance of photon emission around 650 nm with a bandpass filter of 650 ± 20 nm (Figure 2c), which shows that the photon emission maintains the designed propagation angles as well as the corresponding polarizations.

The proposed design approach can be used to design holography metasurfaces for structuring multichannel photon emission propagating at different zenith angles and thus reconstructing the preset signal waves with different quantum light holography. Here, we set the signal waves with the radial polarization and with two set of different zenith angles of $\theta_1 = 20°$ and $\theta_2 = 10°$ and the azimuthal angles (clockwise) of $\varphi_1 = 30°$, $\varphi_2 = 90°$, $\varphi_3 = 150°$, $\varphi_4 = 210°$, $\varphi_5 = 270°$, and $\varphi_6 = 330°$, respectively, keeping the amplitudes of six signal waves being identical (i.e., $|\boldsymbol{E}_{s,1}| = |\boldsymbol{E}_{s,2}| = |\boldsymbol{E}_{s,3}| = |\boldsymbol{E}_{s,4}| = |\boldsymbol{E}_{s,5}| = |\boldsymbol{E}_{s,6}|$). Figure 3a presents the generated metasurface configuration and the corresponding simulation results, demonstrating that photon emission propagates in the designed directions and can also be decomposed into LCP and RCP components. The QE-coupled holography metasurfaces are then fabricated with the preselected ND-NVs, which precisely locate in the center of the structure (Figure 3b). From the experiment results measured with a bandpass filter of 676 ± 15 nm, one can see that photon emission in each channel propagates in the designed direction with a donut-shape intensity profile, which generally coincides well with the simulation results. For the experiment results measured with a bandpass filter of 650 ± 20 nm, similar to those results with the identical zenith angle (Figure 2c), the photon emission in each channel still propagates in the right direction, though they are bright spots rather than donut-shaped intensity profiles. This can be easily understood as it is 20 nm away from the design wavelength and the measured photon emission is broadband, while the design is conducted for a single wavelength (670 nm), nevertheless, it also shows the robustness of the design approach for structuring photon emission into arbitrary angles.

Furthermore, we develop the holography approach in a more general case that can temper multichannel photon emission with different intensities in each channel. By introducing the amplitude factor α_n for the signal waves, i.e., $\alpha_n|\boldsymbol{E}_{s,n}|$, the contribution of each signal wave in the interference process can be modulated, thus changing the binarized configuration. We set the signal waves still with radial polarization and with the zenith angle of $\theta = 20°$ and azimuthal angles (clockwise) of $\varphi_1 = 0°$, $\varphi_2 = 60°$, $\varphi_3 = 120°$, $\varphi_4 = 180°$, $\varphi_5 = 240°$, and $\varphi_6 = 300°$, which is the same condition as the first case, while introducing the amplitude factors of $\alpha_1 = 0.8$, $\alpha_2 = 0.9$, $\alpha_3 = 1$, $\alpha_4 = 1.1$, $\alpha_5 = 1.2$, and $\alpha_6 = 1.3$. As expected, the interference pattern and the binarized metasurface are different with the configuration in Figure 2a that is symmetric. The generated photon emission propagates in designed off-normal angles, most importantly, the intensities gradually increase (clockwise). The designed holography metasurface is precisely fabricated around ND-NVs. Both the experiment results characterized with the bandpass filters of 676 ± 15 and 650 ± 20 nm show the directional photon emission with gradually changed intensity for the total emission patterns (NA = 0.9), the LCP component, and the RCP component. Therefore, the developed VSH approach provides a powerful tool for designing holography metasurfaces to flexibly temper the multichannel QE photon emission with arbitrary directions, polarizations, and intensity ratios. More-

https://doi.org/10.1021/acsphotonics.3c01745
ACS Photonics 2024, 11, 1584−1591

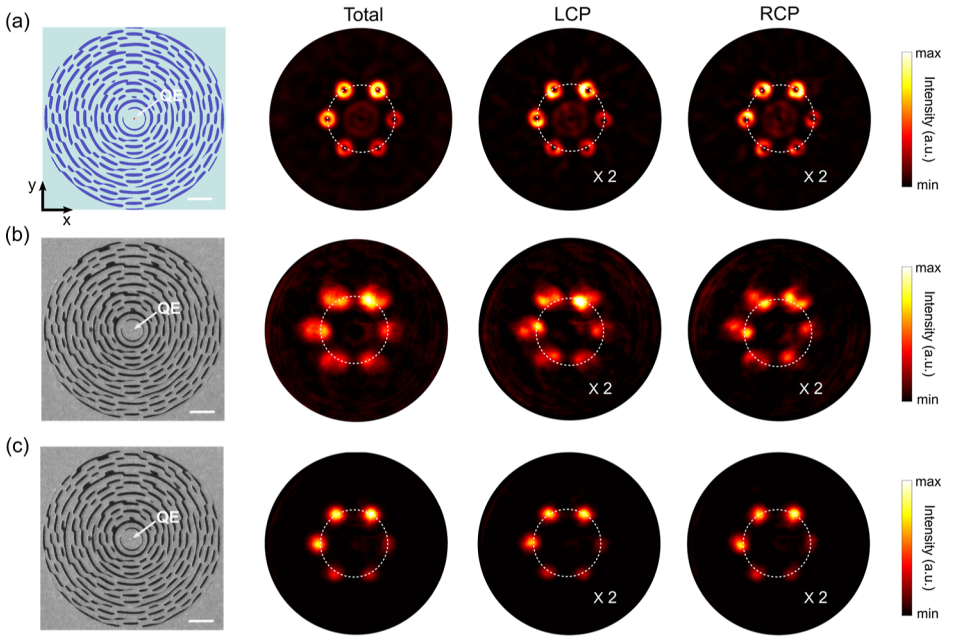

Figure 4. Tempering photon emission into multichannel off-normal directions with the different strength in each channel from on-chip QE-coupled holography metasurfaces. (a) Simulation results of the generation of photon emission propagation with the zenith angle of $\theta = 20°$ and azimuthal angles of $\varphi_1 = 0°$, $\varphi_2 = 60°$, $\varphi_3 = 120°$, $\varphi_4 = 180°$, $\varphi_5 = 240°$, and $\varphi_6 = 300°$, where the intensities gradually increase. From the left to the right: the configuration (scale bar, 2 μm), the emission pattern (NA = 0.9), the LCP component, and the RCP component. (b) Experimental results with a bandpass filter of 676 ± 15 nm. From left to right: the SEM image of the sample (scale bar, 2 μm), the emission pattern (NA = 0.9), the LCP component, and the RCP component. (c) Experimental results with a bandpass filter 650 ± 20 nm.

over, from the spectrum of photon emission (Figure S6), the appearance of NV^- and NV^0 zero phonon lines indicates that the photon emission comes from QE-coupled holography metasurfaces, which maintains the properties of spectral emission of ND-NVs after being integrated with the designed metasurfaces.[15,47]

To more clearly validate the developed VSH approach, Figure 5 presents the results of the quantitative characterization of the strength of QE photon emission in each channel, which are calculated based on the results presented in Figure 4. As aforementioned, the designed amplitude factors of signal waves are set as $\alpha_1 = 0.8$, $\alpha_2 = 0.9$, $\alpha_3 = 1$, $\alpha_4 = 1.1$, $\alpha_5 = 1.2$, and $\alpha_6 = 1.3$, the theoretical results of the reconstructed photon emission intensity in each channel would be α_i^2. As shown in Figure 5, the solid lines are the theoretical results that gradually increase from channel 1 to channel 6, where the photon intensities in all of the channels have been normalized to the highest one (i.e., channel 6). For all the regimes, both the simulation and experiment results, including the total photon emission, the LCP component, the RCP component, coincides well with the theoretical design. The small divergence between the simulation and theory may arise from the imperfections of the binarization of metasurfaces from the interference patterns, especially for the complicated situations with the overlap of several channels. For the experiment results, besides the possible nanofabrication errors of the samples, during the characterization, the photon emission passing through lots of optical components, such as lenses, filters, and reflection mirrors, would distort the performance of the photon emission pattern as well as destabilizing the intensity in each channel. Nevertheless, even with these potential negative factors, the experimental results and simulations explicitly demonstrate the design strategy for precisely tempering photon emission into multiple channels.

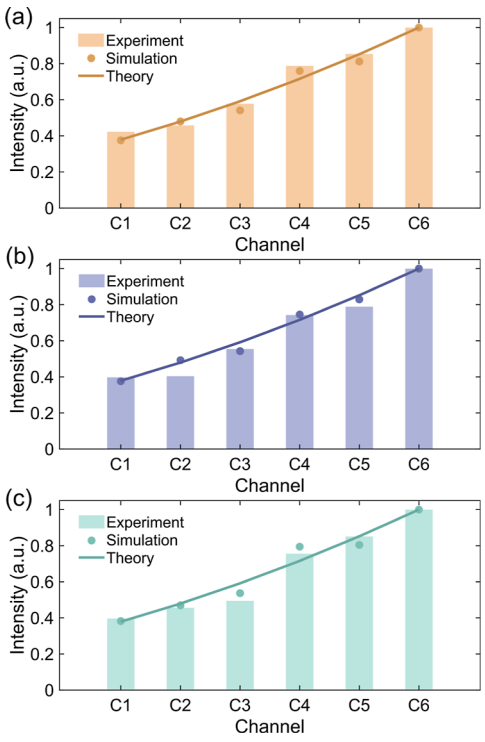

Figure 5. Intensity ratio of the tempered photon emission in each channel from on-chip QE-coupled holography metasurfaces. (a) Photon emission in each channel, (b) LCP component, and (c) RCP component.

CONCLUSIONS

In summary, we have developed the VSH, as an inverse design approach, to flexibly design on-chip emitter-coupled holog-

https://doi.org/10.1021/acsphotonics.3c01745
ACS Photonics 2024, 11, 1584−1591

raphy metasurfaces that can outcouple the nonradiative QE-excited SPPs into multichannel photon emission with desired directions, polarizations, and different intensity ratios in each channel. Based on the proposed approach, we designed, fabricated, and characterized a set of on-chip emitter-coupled holography metasurfaces with different functionalities. We first demonstrated structuring photon emission into six channels with radial polarization and off-normal direction (θ = 20°), followed by realizing the generation of multichannel photon emission with two set of different zenith angles (θ = 10° and θ = 20°). Furthermore, by introducing the varied amplitude factors to the signal waves, thus modulating the interference strength with reference waves, we have realized multichannel photon emission with different intensities in each channel, which coincides well with the theoretical design for both simulation and experiment results. The developed inverse design approach provides a powerful tool to design versatile on-chip emitter-coupled holography metasurfaces to flexibly structure multichannel photon emission with more freedom, including arbitrary directions, polarizations, and intensity ratios, which may find applications in advanced quantum technologies, especially those relevant for high-dimensional quantum information processing.

METHODS

Numerical Simulations. Numerical simulations of characterization of QE-coupled holography metasurfaces are implemented with a 3D FDTD method. The QEs are modeled as vertically orientated electric dipoles with a wavelength of 670 nm, which coincides with the emission peak of ND−NVs at room temperature. The dipole is placed 30 nm on top of the substrate of a silica (20 nm)-covered silver film (150 nm). The metasurfaces are made of dielectric materials with the refractive index being set of 1.41. The thickness of the metasurface is 180 nm. A two-dimensional (x−y) planar monitor is put 100 nm atop the structure, which is utilized for monitoring the electric and magnetic fields that are further used to calculate the far-filed emission patterns, the LCP and RCP components by the near- to far-field transformation projection.

Device Fabrication. The fabrication process of the designed QE-coupled holography metasurfaces follows a well-established sequence of technological steps (Figure S3). First, a 150 nm thick silver film is deposited on the silicon substrate by the thermal evaporation, followed by a 20 nm thick SiO_2 layer being deposited with the magnetron sputtering method. Second, the position markers made of gold are then fabricated on the substrate by a combined process of electron-beam lithography (EBL, JEOL-6490 system, accelerating voltage 30 kV), development, 35 nm thick gold film deposition, and lift-off. Then, the NDs−NVs with proper diluted concentration are spin-coated at 3000 rpm, for 60 s on the substrate surface, after which the NDs−NVs are selected by the precise alignment procedure with the help of the dark-field microscope images. HSQ solution is subsequently spin-coated at 3500 rpm, for 45 s and then being heated at the hot plate on 160 °C for 2 min to form a ∼180 nm layer. Finally, another round of EBL is implemented for fabrication holography metasurfaces on the relative positions of NDs−NVs related to the prefabricated markers. QE-coupled holography metasurfaces are then obtained after the development with the tetramethylammonium hydroxide solution (for 4 min) and water (60 s).

ASSOCIATED CONTENT

Supporting Information

The Supporting Information is available free of charge at https://pubs.acs.org/doi/10.1021/acsphotonics.3c01745.

Detailed descriptions of the developed VSH for tempering multichannel quantum emission; schematic of VSH; evolution of generation of photon emission from single channel to multiple channels; sample fabrication process; schematic of experimental setup; emission pattern with a polarizer; and spectra of three samples (PDF)

AUTHOR INFORMATION

Corresponding Authors

Yinhui Kan − *Center for Nano Optics, University of Southern Denmark, Odense M DK-5230, Denmark;* orcid.org/0000-0001-9798-922X; Email: yk@mci.sdu.dk

Sergey I. Bozhevolnyi − *Center for Nano Optics, University of Southern Denmark, Odense M DK-5230, Denmark;* orcid.org/0000-0002-0393-4859; Email: seib@mci.sdu.dk

Authors

Xujing Liu − *Center for Nano Optics, University of Southern Denmark, Odense M DK-5230, Denmark*

Shailesh Kumar − *Center for Nano Optics, University of Southern Denmark, Odense M DK-5230, Denmark;* orcid.org/0000-0001-5795-0910

Complete contact information is available at: https://pubs.acs.org/10.1021/acsphotonics.3c01745

Author Contributions

Y.H.K. and S.I.B. conceived the idea. Y.H.K. performed theoretical modeling. Y.H.K. fabricated the samples and performed the experimental measurements. Y.H.K., X.J.L., S.K., and S.I.B. analyzed the data. Y.H.K. wrote the manuscript with contributions from all authors.

Notes

The authors declare no competing financial interest.

ACKNOWLEDGMENTS

The authors acknowledge the support from the Natural Science Foundation of Jiangsu Province (BK20210289), the National Natural Science Foundation of China (grant no. 62105150), the European Union's Horizon Europe research and innovation programme under the Marie Skłodowska-Curie Action (grant agreement no. 101064471), the State Key Laboratory of Advanced Optical Communication Systems Networks of China (2022GZKF023), the Villum Experiment from Villum Fonden (grant no. 35950), and the Villum Kann Rasmussen Foundation (Award in Technical and Natural Sciences 2019).

REFERENCES

(1) Buckley, S.; Rivoire, K.; Vučković, J. Engineered Quantum Dot Single-Photon Sources. *Rep. Prog. Phys.* **2012**, *75*, 126503.

(2) Senellart, P.; Solomon, G.; White, A. High-performance semiconductor quantum-dot single-photon sources. *Nat. Nanotechnol.* **2017**, *12*, 1026−1039.

(3) Aharonovich, I.; Englund, D.; Toth, M. Solid-state single-photon emitters. *Nat. Photonics* **2016**, *10* (10), 631−641.

(4) Taminiau, T. H.; Stefani, F. D.; Segerink, F. B.; van Hulst, N. F. Optical antennas direct single-molecule emission. *Nat. Photonics* **2008**, *2* (4), 234−237.
(5) Huck, A.; Kumar, S.; Shakoor, A.; Andersen, U. L. Controlled coupling of a single nitrogen-vacancy center to a silver nanowire. *Phys. Rev. Lett.* **2011**, *106*, 096801.
(6) Wang, J.; Sciarrino, F.; Laing, A.; Thompson, M. G. Integrated photonic quantum technologies. *Nat. Photonics* **2020**, *14*, 273−284.
(7) Hecht, E. *Optics*; Pearson Education: Boston, MA, 2017.
(8) Novotny, L.; Hecht, B. *Principles of Nano-Optics*; Cambridge University Press: Cambridge, 2012.
(9) Kildishev, A. V.; Boltasseva, A.; Shalaev, V. M. Planar photonics with metasurfaces. *Science* **2013**, *339*, 1289.
(10) Yu, N.; Capasso, F. Flat optics with designer metasurfaces. *Nat. Mater.* **2014**, *13*, 139−150.
(11) Solntsev, A. S.; Agarwal, G. S.; Kivshar, Y. S. Metasurfaces for quantum photonics. *Nat. Photonics* **2021**, *15* (5), 327−336.
(12) Qiu, C.-W.; Zhang, T.; Hu, G.; Kivshar, Y. Quo vadis, metasurfaces? *Nano Lett.* **2021**, *21* (13), 5461−5474.
(13) Kan, Y.; Bozhevolnyi, S. I. Advances in metaphotonics empowered single photon emission. *Adv. Opt. Mater.* **2023**, *11*, 2202759.
(14) Komisar, D.; Kumar, S.; Kan, Y.; Wu, C.; Bozhevolnyi, S. I. Generation of radially polarized single photons with plasmonic bullseye antennas. *ACS Photonics* **2021**, *8*, 2190−2196.
(15) Kan, Y.; Andersen, S. K. H.; Ding, F.; Kumar, S.; Zhao, C.; Bozhevolnyi, S. I. Metasurface-enabled generation of circularly polarized single photons. *Adv. Mater.* **2020**, *32*, 1907832.
(16) Wu, C.; Kumar, S.; Kan, Y.; Komisar, D.; Wang, Z.; Bozhevolnyi, S. I.; Ding, F. Room-Temperature on-Chip Orbital Angular Momentum Single-Photon Sources. *Sci. Adv.* **2022**, *8*, No. eabk3075.
(17) Kan, Y.; Ding, F.; Zhao, C.; Bozhevolnyi, S. I. Directional off-normal photon streaming from hybrid plasmon-emitter coupled metasurfaces. *ACS Photonics* **2020**, *7* (5), 1111−1116.
(18) Kumar, S.; Wu, C.; Komisar, D.; Kan, Y.; Kulikova, L. F.; Davydov, V. A.; Agafonov, V. N.; Bozhevolnyi, S. I. Fluorescence enhancement of a single germanium vacancy center in a nanodiamond by a plasmonic Bragg cavity. *J. Chem. Phys.* **2021**, *154*, 044303.
(19) Jia, S.; Li, Y.; Xue, Z.; Chen, K.; Li, Z.; Gong, Q.; Chen, J. Multichannel single-photon emissions with on-demand momentums by using anisotropic quantum metasurfaces. *Adv. Mater.* **2023**, *35*, 2212244.
(20) Wang, K.; Titchener, J. G.; Kruk, S. S.; Xu, L.; Chung, H.-P.; Parry, M.; Kravchenko, I. I.; Chen, Y.-H.; Solntsev, A. S.; Kivshar, Y. S.; et al. Quantum metasurface for multiphoton interference and state reconstruction. *Science* **2018**, *361*, 1104−1108.
(21) Stav, T.; Faerman, A.; Maguid, E.; Oren, D.; Kleiner, V.; Hasman, E.; Segev, M. Quantum entanglement of the spin and orbital angular momentum of photons using metamaterials. *Science* **2018**, *361*, 1101−1104.
(22) Bao, Y.; Lin, Q.; Su, R.; Zhou, Z. K.; Song, J.; Li, J.; Wang, X. H. On-demand spin-state manipulation of single-photon emission from quantum dot integrated with metasurface. *Sci. Adv.* **2020**, *6* (31), No. eaba8761.
(23) Li, L.; Liu, Z.; Ren, X.; Wang, S.; Su, V. C.; Chen, M. K.; Chu, C. H.; Kuo, H. Y.; Liu, B.; Zang, W.; et al. Metalens-array-based high-dimensional and multiphoton quantum source. *Science* **2020**, *368* (6498), 1487−1490.
(24) Solntsev, A. S.; Agarwal, G. S.; Kivshar, Y. S. Metasurfaces for Quantum Photonics. *Nat. Photonics* **2021**, *15*, 327−336.
(25) Curto, A. G.; Volpe, G.; Taminiau, T. H.; Kreuzer, M. P.; Quidant, R.; van Hulst, N. F. Unidirectional emission of a quantum dot coupled to a nanoantenna. *Science* **2010**, *329*, 930−933.
(26) Söllner, I.; Mahmoodian, S.; Hansen, S. L.; Midolo, L.; Javadi, A.; Kiršanskė, G.; Pregnolato, T.; El-Ella, H.; Lee, E. H.; Song, J. D.; Stobbe, S.; Lodahl, P. Deterministic photon-emitter coupling in chiral photonic circuits. *Nat. Nanotechnol.* **2015**, *10*, 775−778.
(27) Andersen, S. K. H.; Kumar, S.; Bozhevolnyi, S. I. Ultrabright linearly polarized photon generation from a nitrogen vacancy center in a nanocube dimer antenna. *Nano Lett.* **2017**, *17*, 3889−3895.
(28) Liu, S.; Vaskin, A.; Addamane, S.; Leung, B.; Tsai, M.-C.; Yang, Y.; Vabishchevich, P. P.; Keeler, G. A.; Wang, G.; He, X.; Kim, Y.; Hartmann, N. F.; Htoon, H.; Doorn, S. K.; Zilk, M.; Pertsch, T.; Balakrishnan, G.; Sinclair, M. B.; Staude, I.; Brener, I. Light-emitting metasurfaces: simultaneous control of spontaneous emission and far-field radiation. *Nano Lett.* **2018**, *18* (11), 6906−6914.
(29) Kan, Y.; Kumar, S.; Ding, F.; Zhao, C.; Bozhevolnyi, S. I. Spin-orbit controlled excitation of quantum emitters in hybrid plasmonic nanocircuits. *Adv. Opt. Mater.* **2020**, *8*, 2000854.
(30) Bogdanov, S. I.; Makarova, O. A.; Xu, X.; Martin, Z. O.; Lagutchev, A. S.; Olinde, M.; Shah, D.; Chowdhury, S. N.; Gabidullin, A. R.; Ryzhikov, I. A.; et al. Ultrafast quantum photonics enabled by coupling plasmonic nanocavities to strongly radiative antennas. *Optica* **2020**, *7* (5), 463.
(31) Chen, B.; Wei, Y.; Zhao, T.; Liu, S.; Su, R.; Yao, B.; Yu, Y.; Liu, J.; Wang, X. Bright solid-state sources for single photons with orbital angular momentum. *Nat. Nanotechnol.* **2021**, *16*, 302−307.
(32) Kan, Y.; Bozhevolnyi, S. I.; Kumar, S. Large spontaneous emission enhancement with silver nanocube dimers on silver substrates. *Adv. Quantum Technol.* **2023**, *6*, 2300196.
(33) Liu, X.; Kan, Y.; Kumar, S.; Komisar, D.; Zhao, C.; Bozhevolnyi, S. I. On-chip generation of single-photon circularly polarized single-mode vortex beams. *Sci. Adv.* **2023**, *9* (32), No. eadh0725.
(34) Liu, X.; Kan, Y.; Kumar, S.; Kulikova, L. F.; Davydov, V. A.; Agafonov, V. N.; Zhao, C.; Bozhevolnyi, S. I. Ultracompact single-photon sources of linearly polarized vortex beams. *Adv. Mater.* **2024**, *36*, 202304495.
(35) Kan, Y.; Bozhevolnyi, S. I. Molding photon emission with hybrid plasmon-emitter coupled metasurfaces. *Adv. Opt. Mater.* **2022**, *10* (12), 2102697.
(36) Komisar, D.; Kumar, S.; Kan, Y.; Meng, C.; Kulikova, L. F.; Davydov, V. A.; Agafonov, V. N.; Bozhevolnyi, S. I. Multiple channelling single-photon emission with scattering holography designed metasurfaces. *Nat. Commun.* **2023**, *14*, 6253.
(37) Kan, Y.; Liu, X.; Kumar, S.; Bozhevolnyi, S. I. Multichannel Quantum Emission with On-Chip Emitter-Coupled Holographic Metasurfaces. *ACS Nano* **2023**, *17* (20), 20308−20314.
(38) Hariharan, P. *Optical Holography*; Cambridge University Press: Cambridge, 1996.
(39) Siampour, H.; Kumar, S.; Bozhevolnyi, S. I. Nanofabrication of Plasmonic Circuits Containing Single Photon Sources. *ACS Photonics* **2017**, *4*, 1879−1884.
(40) Lodahl, P.; Mahmoodian, S.; Stobbe, S. Interfacing single photons and single quantum dots with photonic nanostructures. *Rev. Mod. Phys.* **2015**, *87*, 347−400.
(41) Radulaski, M.; Zhang, J. L.; Tzeng, Y.-K.; Lagoudakis, K. G.; Ishiwata, H.; Dory, C.; Fischer, K. A.; Kelaita, Y. A.; Sun, S.; Maurer, P. C.; et al. Nanodiamond integration with photonic devices. *Laser Photonics Rev.* **2019**, *13*, 1800316.
(42) Iwasaki, T.; Miyamoto, Y.; Taniguchi, T.; Siyushev, P.; Metsch, M. H.; Jelezko, F.; Hatano, M. Tin-Vacancy Quantum Emitters in Diamond. *Phys. Rev. Lett.* **2017**, *119*, 253601.
(43) Aharonovich, I.; Toth, M. Quantum Emitters in Two Dimensions. *Science* **2017**, *358*, 170−171.
(44) Genevet, P.; Capasso, F.; Aieta, F.; Khorasaninejad, M.; Devlin, R. Recent advances in planar optics: from plasmonic to dielectric metasurfaces. *Optica* **2017**, *4*, 139−152.
(45) Sun, S.; Zhou, Z.; Zhang, C.; Gao, Y.; Duan, Z.; Xiao, S.; Song, Q. All-Dielectric Full-Color Printing with TiO_2 Metasurfaces. *ACS Nano* **2017**, *11*, 4445−4452.
(46) Zhan, A.; Colburn, S.; Trivedi, R.; Fryett, T. K.; Dodson, C. M.; Majumdar, A. Low-Contrast Dielectric Metasurface Optics. *ACS Photonics* **2016**, *3*, 209−214.
(47) Bradac, C.; Gaebel, T.; Naidoo, N.; Sellars, M. J.; Twamley, J.; Brown, L. J.; Barnard, A. S.; Plakhotnik, T.; Zvyagin, A. V.; Rabeau, J.

https://doi.org/10.1021/acsphotonics.3c01745
ACS Photonics 2024, 11, 1584−1591

R. Observation and control of blinking nitrogen-vacancy centres in discrete nanodiamonds. *Nat. Nanotechnol.* **2010**, *5* (5), 345−349.

https://doi.org/10.1021/acsphotonics.3c01745
ACS Photonics 2024, 11, 1584−1591